

Molecular and Cellular Characterization of the Biological Effects of Ruthenium(II) Complexes Incorporating 2-Pyridyl-2-pyrimidine-4-carboxylic Acid

Vanessa Pierroz,^{†,‡} Tanmaya Joshi,[§] Anna Leonidova,[†] Cristina Mari,[†] Julia Schur,^{||} Ingo Ott,^{||} Leone Spiccia,^{*,§} Stefano Ferrari,^{*,‡} and Gilles Gasser^{*,†}

[†]Institute of Inorganic Chemistry, University of Zurich, Winterthurerstrasse 190, CH-8057 Zurich, Switzerland

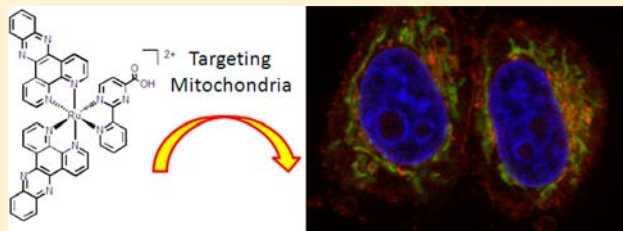
[‡]Institute of Molecular Cancer Research, University of Zurich, Winterthurestrasse 190, CH-8057 Zurich, Switzerland

[§]ARC Centre of Excellence for Electromaterials Science and School of Chemistry, Monash University, Victoria 3800, Australia

^{||}Institute of Medicinal and Pharmaceutical Chemistry, Technische Universität Braunschweig, Beethovenstrasse 55, 38106 Braunschweig, Germany

S Supporting Information

ABSTRACT: A great majority of the Ru complexes currently studied in anticancer research exert their antiproliferative activity, at least partially, through ligand exchange. In recent years, however, coordinatively saturated and substitutionally inert polypyridyl Ru(II) compounds have emerged as potential anticancer drug candidates. In this work, we present the synthesis and detailed characterization of two novel inert Ru(II) complexes, namely, $[\text{Ru}(\text{bipy})_2(\text{Cpp-NH-Hex-COOH})]^{2+}$ (**2**) and $[\text{Ru}(\text{dppz})_2(\text{CppH})]^{2+}$ (**3**) (bipy = 2,2'-bipyridine; CppH = 2-(2'-pyridyl)pyrimidine-4-carboxylic acid; Cpp-NH-Hex-COOH = 6-(2-(pyridin-2-yl)pyrimidine-4-carboxamido)hexanoic acid; dppz = dipyrido[3,2-a:2',3'-c]phenazine). **3** is of particular interest as it was found to have IC_{50} values comparable to cisplatin, a benchmark standard in the field, on three cancer cell lines and a better activity on one cisplatin-resistant cell line than cisplatin itself. The mechanism of action of **3** was then investigated in detail and it could be demonstrated that, although **3** binds to calf-thymus DNA by intercalation, the biological effects that it induces did not involve a nuclear DNA related mode of action. On the contrary, confocal microscopy colocalization studies in HeLa cells showed that **3** specifically targeted mitochondria. This was further correlated by ruthenium quantification using High-resolution atomic absorption spectrometry. Furthermore, as determined by two independent assays, **3** induced apoptosis at a relatively late stage of treatment. The generation of reactive oxygen species could be excluded as the cause of the observed cytotoxicity. It was demonstrated that the mitochondrial membrane potential in HeLa was impaired by **3** as early as 2 h after its introduction and even more with increasing time.



The image shows the chemical structure of a ruthenium(II) complex on the left, which is a polypyridyl complex with a central Ru(II) center coordinated to two bipyridine (bipy) ligands and one Cpp-NH-Hex-COOH ligand. A red arrow points from the complex to a confocal microscopy image on the right. The microscopy image shows two cells with blue nuclei and green/yellow signals indicating mitochondrial targeting. The text 'Targeting Mitochondria' is written above the arrow.

INTRODUCTION

The phenomenal success of the chemotherapeutic drug cisplatin has boosted the research directed at novel metal-based drugs, especially since severe side effects including nephrotoxicity can be encountered during treatment with this compound.^{1–7} Among the potential metal-based candidates, ruthenium complexes have emerged as leading players by showing extremely promising results.^{8–18} Two Ru(III) candidates, namely, imidazolium *trans*-[tetrachloro-(dimethylsulfoxide)-(1*H*-imidazole)ruthenate(III)] (NAMI-A)^{19,20} and indazolium *trans*-[tetrachlorobis(1*H*-indazole)-ruthenate(III)] (KP1019),²¹ have even entered clinical trials (Figure 1).²² Despite their structural similarities, these two Ru complexes exert their cytotoxic action differently. While KP1019 exhibits promising effects against a variety of tumor models including colorectal carcinomas and primary explanted human tumors,²³ NAMI-A only has a minor activity against primary tumor cells but an impressive efficacy against the

formation of metastases.^{23,24} For both NAMI-A and KP1019, and generally speaking for the majority of the Ru complexes investigated for medicinal purposes, the complexes usually undergo ligand exchange to exert their antiproliferative activities, as cisplatin does. There are, however, exceptions such as the Ru(II) based enzyme inhibitors of Meggers et al.^{25–27} and the coordinatively saturated and substitutionally inert polypyridyl Ru(II) compounds.^{28,29} For the latter, the cytotoxic effects were at least partially attributed to noncovalent interactions with nucleic acids, particularly DNA.^{30–37} In recent years, however, several studies have shown that other factors, such as modification of cell membrane and cell adhesion properties,³⁸ topoisomerase I and II inhibition³⁹ or mitochondria-mediated apoptosis,^{32,33,40–43} could be responsible for cytotoxicity.

Received: July 25, 2012

Published: November 27, 2012

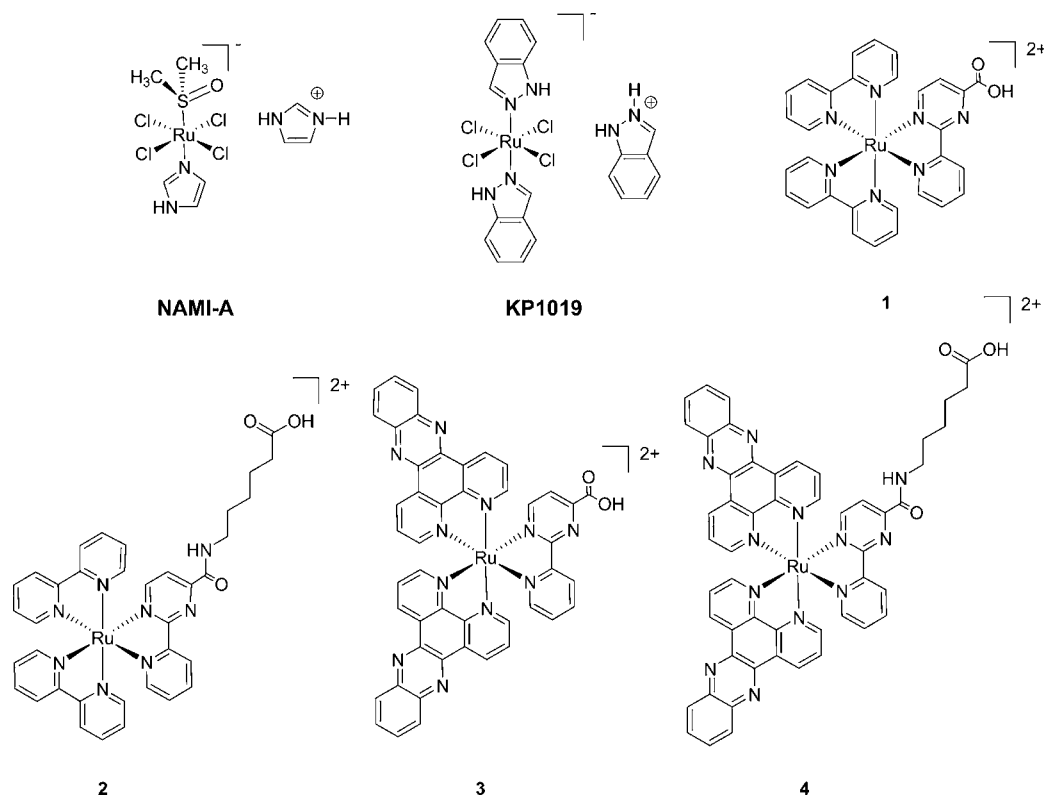
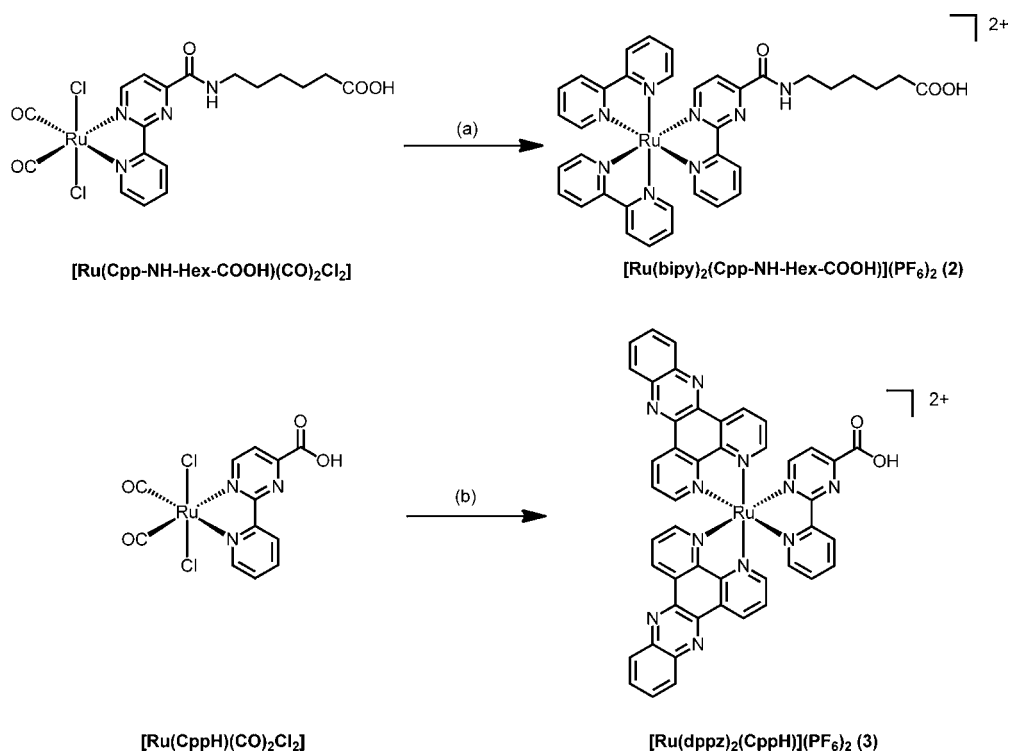


Figure 1. Structures of NAMI-A, KP1019, and the Ru(II) complexes (isolated as hexafluorophosphate salts) studied in this work.

Scheme 1. Syntheses of 2 and 3^a



^aConditions: (a) (i) bipy, Me₃NO, 2-methoxyethanol, Δ, 4 h; (ii) CH₃CN/H₂O/H₂SO₄ (45:45:10), Δ, 24 h, 75%; (b) (i) dppz, Me₃NO, 2-methoxyethanol, Δ, 4 h; (ii) CH₃CN/H₂O/H₂SO₄ (45:45:10), Δ, 24 h, 66%.

Inspired by these findings, we have decided to thoroughly investigate the *in vitro* behavior of four Ru(II) complexes bearing a derivative of the 2-(2'-pyridyl)pyrimidine (Cpp)

ligand,⁴⁴ namely, [Ru(bipy)₂(CppH)]²⁺ (**1**),⁴⁴ [Ru(bipy)₂(Cpp-NH-Hex-COOH)]²⁺ (**2**), [Ru(dppz)₂(CppH)]²⁺ (**3**), and [Ru(dppz)₂(Cpp-NH-Hex-COOH)]²⁺ (**4**)⁴⁵ (bipy =

Table 1. Cytotoxicities (IC₅₀) of 1–4 Dequalinium Chloride Hydrate and Cisplatin towards Human (Cancer) Cell Lines^a

| | IC ₅₀ (μM) | | | | | |
|------------------------------|-----------------------|------------|------------|------------|------------|------------|
| | HeLa | MCF7 | U2OS | A2780 | A2780-CP70 | MRC-5 |
| 1 | >100 | >100 | >100 | >100 | >100 | >100 |
| 2 | >100 | >100 | >100 | >100 | >100 | >100 |
| 3 | 10.0 ± 1.3 | 4.3 ± 0.1 | 13.5 ± 2.5 | 2.8 ± 0.1 | 4.0 ± 1.2 | 15.1 ± 2.2 |
| 4 | 57.5 ± 4.8 | 22.0 ± 3.8 | 83.2 ± 5.6 | 26.8 ± 7.6 | 49.6 ± 5.0 | 66.3 ± 8.1 |
| cisplatin | 11.5 ± 2.9 | 1.8 ± 0.3 | 11.8 ± 1.7 | 2.9 ± 0.6 | 13.8 ± 3.0 | 7.9 ± 1.2 |
| dequalinium chloride hydrate | 21.9 ± 3.6 | 2.9 ± 0.5 | 13.4 ± 2.5 | 1.0 ± 0.1 | 1.7 ± 0.7 | 48.9 ± 7.6 |

^aCells were treated with different concentrations of the ruthenium complexes, cisplatin, and dequalinium chloride hydrate for 48 h. The cell viability was determined by using the resazurin reduction test.

2,2'-bipyridine; CppH = 2-(2'-pyridyl)pyrimidine-4-carboxylic acid; Cpp-NH-Hex-COOH = 6-(2-(pyridin-2-yl)pyrimidine-4-carboxamido)hexanoic acid; dppz = dipyrido[3,2-*a*:2',3'-*c*]-phenazine) (Figure 1). Complex 4 was recently prepared in our laboratories with a view to the development of electrochemiluminescent Ru(II)-peptide nucleic acid bioconjugates as either DNA/RNA biosensors or cellular uptake enhancers.^{45–47} Herein, we also describe the synthesis and characterization of the two Ru(II) complexes 2 and 3 (Figure 1), including the X-ray crystal structure of 2. This work, to the best of our knowledge, presents one of the most detailed biological evaluations of a polypyridyl Ru(II) complex, 3, which was found extremely cytotoxic on different cancer cell lines.

RESULTS AND DISCUSSION

Synthesis and Characterization of the Ru(II) Complexes. The two Ru(II) complexes 1 and 4 presented in Figure 1 were prepared as previously reported by our groups.^{44,45} Compounds 2 and 3 were synthesized in an analogous manner by reacting [Ru(Cpp-NH-Hex-COOH)(CO)₂Cl₂]⁴⁵ and [Ru(CppH)(CO)₂Cl₂]⁴⁴ with bipy and dppz, respectively (Scheme 1). All Ru(II) complexes were unambiguously characterized by ¹H NMR spectroscopy, ESI mass spectrometry, and elemental analysis (see Experimental Section for further details and Figures S1–S4 in Supporting Information for the ¹H NMR spectra of 2 and 3 as well as the absorption and emission spectra of 1–4).

X-ray Crystal Structures. During the preparation of 1–4, single crystals of 1 and 2 were obtained and their structures were elucidated by X-ray crystallography. The asymmetric unit (ASU) of 1 consists of a [Ru(bipy)₂(CppH)]²⁺ cation, hexafluorophosphate anions, and noncoordinated water molecules (Figure S5 in the Supporting Information) {A related structure in which the CppH ligand is deprotonated was published recently by our group.⁴⁴ As for 1, a [Ru(bipy)₂(Cpp-NH-Hex-COOH)]²⁺ unit, perchlorate counteranions, and noncoordinated water molecules define the ASU for 2 (Figure S6 in the Supporting Information). The X-ray structural analysis showed Ru(II) center to reside in a distorted octahedral geometry in both complexes, with bond distances and angles typical of Ru(II) diimine complexes.^{44,48} The *trans*-N–Ru–N angles and N–Ru–N bite angles, formed between the nitrogen atoms of the 2,2'-bipyridine and 2-(2'-pyridyl)pyrimidine (Cpp) rings and the Ru(II) center, are in the typical range (172.29(14)–175.40(13)° and 78.60(15)–79.03(14)°, respectively), as reported for other tris(diimine)Ru(II) complexes (Table S1 in Supporting Information).^{44,48} Coordination of the Cpp unit to the Ru(II) center in 1 and 2 involves the N4 and N3 nitrogen atoms and the carboxylate group points away from the Ru(II) center as previously observed for

other Ru(II)-2-(2'-pyridyl)pyrimidine-4-carboxylic acid complexes.⁴⁴ The crystal structure for 2 (see Figure S7 in the Supporting Information) also shows hydrogen-bonding of the N–H and O–H (protonated carboxylate) groups with the perchlorate counteranions present in the crystal lattice along with C–H...π interactions between the aromatic protons and π-electron rich bipyridyl ring.

Cytotoxicity Studies. The cytotoxicity of complexes 1–4 toward human cervical cancer HeLa, breast carcinoma MCF7, osteosarcoma U2OS, ovarian carcinoma A2780, and cisplatin-resistant ovarian carcinoma A2780-CP70 cell lines was investigated using a fluorometric cell viability assay (Resazurin).⁴⁹ As a control, the toxicity of the compounds was also tested toward human lung fibroblasts MRC-5. Furthermore, for the purposes of comparison the toxicities of cisplatin and dequalinium chloride hydrate, a known antiproliferative compound with a mitochondrial implication in cell death,^{50,51} were also determined on the same cell lines (see Figures S8–S10 in the Supporting Information for the graphs of the Resazurin assays of compound 3, cisplatin and dequalinium chloride hydrate). As shown in Table 1, the Ru(II) bipyridyl derivatives 1 and 2 did not present cytotoxicity in any of the cell lines tested. These observations are in contrast to the results obtained for the Ru(II) dppz derivatives 3 and 4, which were cytotoxic toward all the six cell lines employed in this study. Of particular interest is the observation that the IC₅₀ values determined for 3 are close, or even lower, than those for cisplatin and in a similar range to dequalinium chloride hydrate. Notably, 3 was found to be more active on a cisplatin-resistant cell line than cisplatin itself, an observation that points to its therapeutic potential, particularly in light of the worrying emergence of cisplatin resistance in tumors.⁵² Moreover, the finding that 3 was found to be less cytotoxic than cisplatin on the healthy cell line studied in this work is suggestive of a better therapeutic profile than cisplatin. Another striking result is that 4, the structurally similar derivative of 3, displayed much higher IC₅₀ values than 3 (>12-fold on the A2780 cell line). This rather surprising finding clearly indicates that subtle structural changes have an important impact on the toxicity and prompted us to further investigate the origin of this behavior.

Cellular Localization. As a first step toward elucidating the mechanism of action of 3, the favorable photophysical properties of 1–4 have been used to evaluate their localization in HeLa cells. It was anticipated that the cellular localization of the complexes bearing the dppz moieties (3 and 4) could be possible if they were directed to a hydrophobic environment as the fluorescence of these compounds is quenched in aqueous media. On the contrary, the fluorescence properties of 1 and 2 should not be so significantly solvent-dependent and it was expected that they could be detected in any cellular

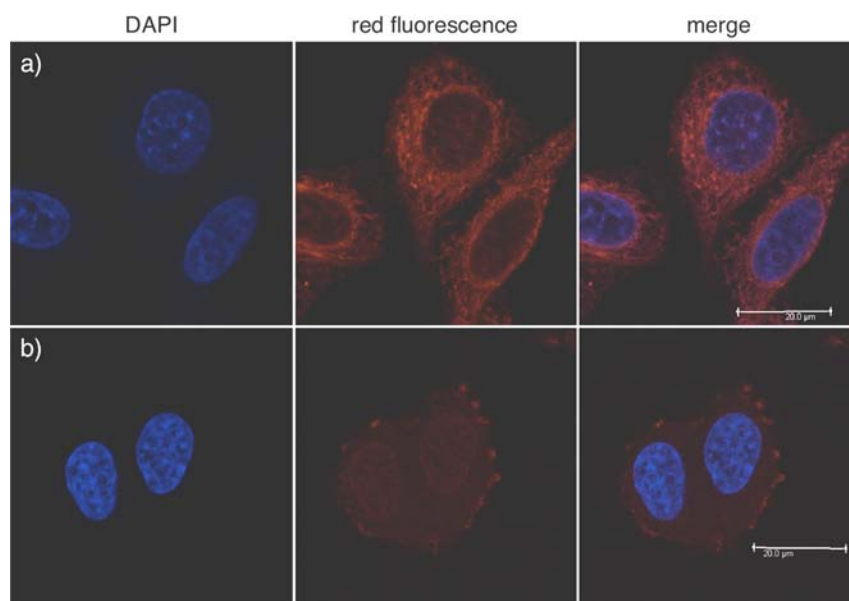


Figure 2. Fluorescence confocal microscopy images of HeLa cells incubated with (a) **3** ($20\ \mu\text{M}$) and (b) **4** ($60\ \mu\text{M}$) for 2 h. Images show DAPI staining, cellular staining of ruthenium compounds, and the overlay.

compartments. The localization of the complexes was then assessed by fluorescence microscopy (see Figure S11 in the Supporting Information). The presence of **1** and **2** in living cells or after fixation in formaldehyde was very difficult to evaluate. Only a weak fluorescence could be detected which we have assumed indicates that these compounds were poorly taken up by the cells. However, very clear confocal microscopy images were obtained for **3** and **4** after cell fixation with formaldehyde (Figure 2). The most important finding to emerge from these studies is that, even though **3** and **4** are structurally quite similar, their cellular localization was extremely different. Compound **4** diffused throughout the cell, including the nucleus. In addition, the outer cellular membrane also seemed to be a primary target of **4**. On the contrary, **3** localized mainly to the cytoplasm with only weak fluorescence detectable in the nucleus. This significant difference in localization is likely to be responsible for the disparity in cytotoxicity observed for these Ru(II) complexes. To obtain further information on the exact localization of **3**, colocalization experiments were performed. Mitotracker green FM was employed for this purpose as it was anticipated that **3** could be localized in the mitochondria. As shown in Figure 3, an excellent superimposition pattern between the commercially available dye and **3** could be observed (see also the online video in Supporting Information). To the best of our knowledge, there are only a handful of reports which so clearly demonstrate by fluorescence microscopy that mitochondria are the target of inert polypyridyl Ru complexes,^{40,41,53} although these organelles have only recently been considered as target of such compounds.^{32,33,40–42,54} Of particular relevance here is the fact that mitochondria are critical targets of cytotoxic gold compounds.^{55–59}

As **3** mainly exhibits fluorescence in a hydrophobic environment, it could also be localized in another cellular organelle hampering visualization by fluorescence microscopy. High-resolution continuum source atomic absorption spectrometry (HR-CS AAS) is an analytical method of choice in this situation, as it allows the detection of trace metal concentrations in biological tissues.^{60–62} In previous studies,

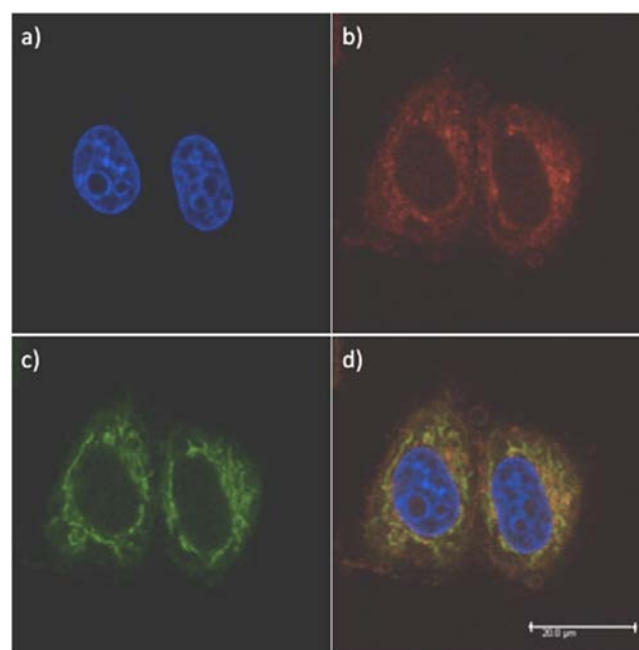


Figure 3. Fluorescence confocal microscopy images of HeLa cells incubated with **3** ($20\ \mu\text{M}$) for 2 h and Mitotracker green FM for 45 min: (a) DAPI staining; (b) cellular staining of **3**; (c) Mitotracker green FM staining; and (d) the overlay image.

it has been reported that the amount of ruthenium taken up by cancer cells can be a deciding factor in obtaining active ruthenium compounds.^{33,38,63} In this study, we decided to go one step further by endeavoring to ascertain that **3** mainly targets mitochondria. Therefore, we incubated HeLa cells with $50\ \mu\text{M}$ of **3** for 2 h and isolated the mitochondria from the cells. The uptake of **3** into whole cells and into their mitochondrial fractions was quantified by determination of the ruthenium content by HR-CS AAS (Figure 4). The cellular and mitochondrial protein content of the same samples was determined by the method of Bradford⁶⁴ and the measured

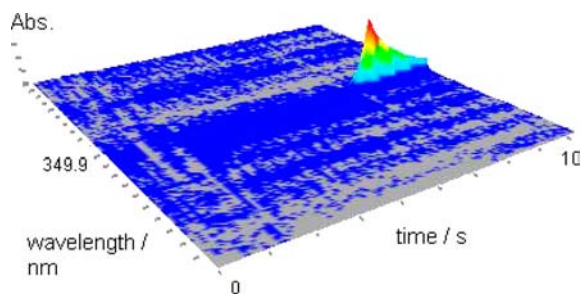


Figure 4. Ruthenium absorption signal of a mitochondrial fraction measured by HR-CS AAS.

ruthenium levels were correlated to the respective protein content. The analysis revealed a high mitochondrial uptake of **3** with a concentration of 29.3 nmol Ru/mg mitochondrial protein. This corresponds to 68% of the total cellular uptake of **3** into HeLa cells.

All in all, fluorescence microscopy and high-resolution continuum source atomic absorption spectrometry indicate that uptake into the mitochondria may be a major pathway for the biodistribution of **3**.

Stability in Human Plasma. To determine whether **3** was stable in biological media, its stability in human plasma was assessed following an experimental protocol that we have recently used in the study of ferrocenyl derivatives.⁶⁵ As clearly evident from the LC–MS traces (Figure S12 and Table S2 in the Supporting Information), **3** shows no significant decomposition in human plasma when monitored over a period of three days. This observation is an excellent indication that the intact Ru(II) complex is responsible for the observed cytotoxic activity.

Cellular Uptake Mechanism. To obtain more insight into the mechanism of the cellular entry of compound **3**, we first assessed whether cellular uptake is energy dependent. As nicely explained in a recent review by Pucket and Barton,⁶⁶ endocytosis and active transport proteins require energy while passive diffusion through the membrane and diffusion are energy independent. In this respect, **3** was incubated into HeLa cells at 4, 23, and 37 °C for 6 h, and the relative uptake of **3** was assayed by flow cytometry (see Figure S13 in the Supporting Information). As shown in Figure S14a in the Supporting Information, the uptake of **3** increased with temperature, indicating that it was energy-dependent. With no significant perturbation observed in mitochondrial membrane potential of untreated HeLa cells between 4 and 37 °C (Supporting Information, Figure S14b), it implies that the uptake of **3** into HeLa cells is not only due to passive diffusion as it could have been first anticipated.

Distribution Coefficient (logD) and Electrochemical Studies. The lipophilicity of a compound is well-known to have a strong influence on its cellular uptake and localization,^{66–68} and it has been shown that lipophilic cations accumulate in mitochondria as a result of the negative potential difference across the mitochondrial membrane.^{66,69,70} With this in mind, we have evaluated the lipophilicity of the Ru complexes by determining the distribution coefficients at pH = 7.01, a good approximation of physiological conditions, using the “shake-flask” method. The distribution coefficient (logD) is a measure of partitioning of a compound, in its ionized form, between organic and water phases, and consequently it is pH dependent. As shown in Table 2, compounds **3** and **4** are the most lipophilic compounds of the series due to the presence of

Table 2. Distribution Coefficients between Octanol and Phosphate Buffer 10 mM (pH 7.01) Obtained Using the “Shake-Flask” Method and Midpoint Potentials (E_m)^a Determined from Cyclic Voltammetry at a Glassy Carbon Electrode Using a Scan Rate of 100 mV s⁻¹ in MeCN (0.1 M nBu₄NPF₆) at (20 ± 2) °C

| | logD _{7.01} ^b | E_m /mV |
|----------|-----------------------------------|-------------------|
| 1 | -1.81 | 980 ⁴⁴ |
| 2 | -1.58 | 970 |
| 3 | -0.21 | 1100 |
| 4 | -0.05 | 1065 |

^aMidpoint potential = $E_m = (E_p^{ox} + E_p^{red})/2$, quoted versus Fc^{0/+}
^bComplex concentrations range between 37 and 50 μM.

the two dppz ligands. Of note, the logD_{7.01} values correlate well with the solubility of **1–4** in buffer, namely, **1** and **2** are comparatively more soluble in buffer than **3** and **4** (up to 50 μM). As expected, addition of an alkyl chain in **2** and **4** also increases the lipophilicity of the compounds compared to the parent compounds **1** and **3**, respectively.

To evaluate whether a correlation exists between the electrochemical behavior of the Ru complexes and their cytotoxicities, the midpoint potentials E_m for the Ru(II)/Ru(III) couple of **2–4**, namely, the average of the oxidation and reduction peak potentials, were determined from the cyclic voltammograms (see Table S3 and Figures S15–S18 in Supporting Information). The E_m values are equal to the reversible potentials, provided the diffusion coefficient of the oxidized Ru(III) and reduced Ru(II) form are equal. Although the E_m values of the compounds are similar, complex **3**, which is the hardest to oxidize, is the most cytotoxic compound of the series. However, there is no clear trend between the potential and cytotoxicity. As expected, the oxidation process is diffusion controlled (plot of peak current vs scan rate is linear), as is generally the case with tris(diimine) Ru(II) complexes,^{45,46,48} and diffusion coefficients of **1–4** could be determined (see Table S3 in the Supporting Information) by applying the Randles–Sevcik relationship.^{71–73}

DNA and Protein Binding Experiments. The ability of transition metal polypyridyl complexes to reversibly bind DNA through intercalation or groove binding is well documented.^{74–76} Depending on the type of metal complexes, this feature was employed to develop imaging agents in living cells.⁷⁷ As mentioned in the introduction, however, non-covalent binding to DNA of these coordinatively saturated and substitutionally inert polypyridyl Ru(II) compounds was also assumed to be responsible for the cytotoxic effects observed for some of these complexes. We therefore investigated the binding of complexes **3** and **4** to calf-thymus DNA (CT-DNA).^{78,79} The absorption spectra shown in Figures S19 and S20 in the Supporting Information confirm an intercalative mode of DNA binding for **3** and **4** rather than groove binding or electrostatic binding interactions. A significant change in absorbance (hypochromism for **3** and **4** as well as a supplementary red shift for **4**) ascribable to stacking of the aromatic chromophore between the DNA nucleobase pairs is indeed noticed.⁷⁶ In comparison, as expected, no change in absorption is observed for complexes **1** and **2** (Figures S21 and S22 in the Supporting Information). The intrinsic binding constants (K_b) for intercalation of **3** and **4** into DNA were obtained by fitting the absorption and emission titrations data to the non-cooperative model for DNA binding^{80–82} (Figures S23 and

Table 3. DNA Binding Constants Obtained by DNA Titrations of All the Complexes in Phosphate Buffer at pH 7.01^a

| | absorbance data | | emission data | |
|---|---|----------------------|---|----------------------|
| | K_b (M^{-1} per nucleotide) | binding site size(s) | K_b (M^{-1} per nucleotide) | binding site size(s) |
| 3 | $(3.95 \pm 0.40) \times 10^6$ (at 364 nm) | 1.25 ± 0.30 | $(2.13 \pm 0.60) \times 10^6$ (at 628 nm) | 1.17 ± 0.10 |
| 4 | $(9.29 \pm 0.60) \times 10^6$ (at 364 nm) | 0.65 ± 0.05 | $(2.47 \pm 0.40) \times 10^6$ (at 623 nm) | 0.89 ± 0.03 |
| [Ru(L)(dppz) ₂] ⁴⁺ 85 | $(2.2 \pm 0.5) \times 10^6$ (at 447 nm) | 1.2 | NA ^b | NA ^b |
| [Ru(bipy) ₂ dppz] ²⁺ 81 | 2.9×10^6 (at 369 nm) | 0.84 | 1×10^7 | 0.95 |

^aMeasurement buffer contained 10 mM phosphate buffer and 50 mM NaCl. Abbreviations: L = 5,5'-di(1-(trimethylammonio)methyl)-2,2'-dipyridyl cation; bipy = 2,2'-bipyridine; dppz = dipyrido[3,2-*a*:2',3'-*c*]phenazine]. ^bNot Available.

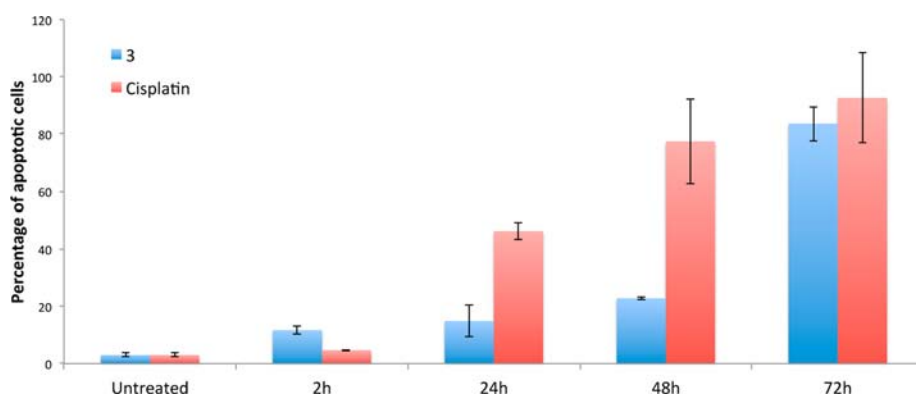


Figure 5. Quantification of apoptotic cells using the YO-PRO assay. HeLa cells were incubated with 3 (20 μ M) and cisplatin (20 μ M) for 2, 24, 48, or 72 h at 37 $^{\circ}$ C.

S24 in Supporting Information) and are presented in Table 3. The obtained values ($>10^6 M^{-1}$ range) indicate a high binding affinity for DNA and correlate well with other dppz-containing Ru(II) complexes (Table 3). The less than unity binding site size(s) obtained from the K_b fits for 4 also shows an extent of cooperativity for intermolecular stacking of the dppz ligands on the DNA surface.^{83,84} Such π -stacking and aggregation of cationic Ru(II) complex can be further facilitated by polyanionic DNA backbone.⁸³ The stronger binding of 4, compared to 3, was further examined by DNA gel experiments (Figure S25 in the Supporting Information), which revealed a stronger interaction with DNA for 4 than for 3. Thus, a contribution from such surface aggregation of 4 on DNA surface to its binding affinity cannot be ruled out. Given that the charge of the two complexes at pH = 7.0 is identical (+1), we speculate that the slightly higher binding affinity for 4 could be reflecting the ability of the more “flexible” anionic carboxylate group in 4 to hydrogen-bond with protons present on the DNA, and its slightly greater hydrophobicity. As proteins can be the targets of metallo-drugs,²⁷ we incubated the ruthenium complexes with proteins of varying molecular weight resolved by SDS-polyacrylamide gel electrophoresis (Figure S26 in the Supporting Information). Similar to DNA, complex 4 was found to bind more strongly to the proteins than 3. A possible explanation to this observation could be that the carboxylate group in 4 is likely to bind more to protonated amino acids due to its “flexibility”. Regardless of the origin of the greater binding affinity of 4, it is important to highlight the fact that the most cytotoxic compound is not the one binding most strongly to DNA or proteins.

Mechanism of Cytotoxicity. To assess whether 3 causes cell death by apoptosis or necrosis, the YO-PRO and the annexin-V assays were performed. For the former, cytofluorometric analysis of programmed cell death (apoptosis) allows detection of cell membrane permeabilization, an event taking place during apoptosis.⁸⁶ Hence, HeLa cells were treated with 20 μ M of either 3 or cisplatin for 2, 24, 48, or 72 h before being incubated with the dye YO-PRO (2.5 μ M). As shown in Figure 5, 3 does induce apoptosis during the first 48 h but only slightly, with the percentage of apoptotic cells increasing by a factor of ~ 5 after 72 h. In comparison, cisplatin induced apoptosis in a more gradual manner. The data showed that, after 48 h of treatment with 3 at a dose corresponding to the IC_{50} , only 20% of the cells were apoptotic, indicating that apoptosis is triggered at a later stage. As expected, the annexin-V assay confirmed the results obtained with the YO-PRO assay as it was again found that 3 induced apoptosis (see Figure S27 in the Supporting Information). In the case of the annexin-V assay, apoptosis was found to occur at a slightly faster rate than for the YO-PRO assay.

To clarify the mechanism by which 3 induces apoptosis, the activity of caspases 3/7 was examined using the Caspase-Glo 3/7 assay. These caspases are known to be the apoptosis executors, to which extrinsic and intrinsic pathway converge.⁸⁷ The data showed a higher caspase activity upon incubation of cells with 3 (20 μ M, 24 h). The low-specificity kinase inhibitor staurosporin (150 nM, 6 h) was used as positive control, confirming that 3 induced cell death by apoptosis (see Figure S28 in the Supporting Information).

Another important factor which could explain the cytotoxicity exerted by 3 is the production of reactive oxidative species

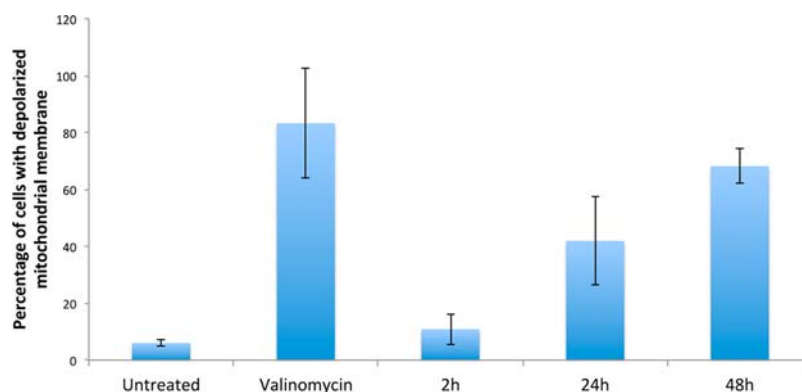


Figure 6. Effect of **3** (20 μM) on the mitochondrial membrane potential in HeLa cells. Cells were treated for 2, 24, or 48 h with **3** at 37 $^{\circ}\text{C}$ and the percentage of cells with depolarized mitochondrial membrane was determined. Valinomycin treatment was taken as positive control.

(ROS). This was recently observed with ruthenium-Norharman and ruthenium β -carboline complexes as well as ruthenium containing bis-benzimidazole derivatives complexes.^{32,33,88} In this respect, HeLa cells were treated with **3** in the presence or absence of *N*-acetylcysteine (NAC), which is known to scavenge ROS. As can be seen in Figure S29 in the Supporting Information, ROS were not produced during treatment with **3** at concentrations up to 2-fold the IC_{50} .

Very recently, Meggers, Xu, Wong, Zheng and co-workers reported that Ru(II) complexes could induce cell death by interfering with the membrane potential finally leading to cell apoptosis.^{32,33,40,42,43,88} To assess whether **3** displays a similar behavior, the mitochondrial membrane potential ($\Delta\Psi_{\text{m}}$) was evaluated in HeLa using JC-1 (5,5',6,6'-tetrachloro-1,1',3,3'-tetraethylbenzimidazolylcarbocyanine iodide) and valinomycin as positive control. As shown in Figure 6, the impairment induced by **3** (which is reflected in $\Delta\Psi_{\text{m}}$) is clearly time-dependent (see Figure S30 in Supporting Information for the flow cytometry dot blots). On the contrary, within the temperature range investigated and considering that complex **3** affects the mitochondrial membrane potential of HeLa cells only at 37 $^{\circ}\text{C}$ (see Figure S31 in Supporting Information), a similar clear-cut trend in its temperature-dependent behavior cannot be perceived. It can be postulated that the hydrophobic dppz moieties of **3** intercalate into the mitochondria membrane, thus impairing its potential. This, in turn, leads to the release of the mitochondrial cytochrome c, that induces cell permeabilization and apoptosis.

CONCLUSIONS

After platinum complexes, ruthenium compounds are the most advanced metal-based anticancer drug candidates in medicinal inorganic chemistry with two complexes, namely, NAMI-A²⁴ and KP1019,²¹ already in clinical trials. However, for nearly all ruthenium anticancer agents studied, a ligand exchange, often with a biomolecule, is required for the antiproliferative activity. In this study, we demonstrate that coordinatively saturated and substitutionally inert polypyridyl Ru(II) compounds like **3** can be also very effective as anticancer drug candidates by presenting one of the most detailed biological studies of a cytotoxic inert Ru(II) complex. We could show, with **3** and **4** as examples, that subtle structural changes can have a significant impact on both the cytotoxicity and cellular localization. Using two different techniques, namely, confocal microscopy and atomic absorption spectrometry, **3** was shown to accumulate in mitochondria. This correlation provides solid evidence for the

mechanism of action proposed in this study. Interestingly, while **3** was found to have IC_{50} values relatively close to those of the well-known cisplatin on three cancer cell lines, and to be more active on a cisplatin-resistant cell line than cisplatin itself, **4** presented significantly higher IC_{50} values. We have also demonstrated that **3** exerted its toxicity through a mitochondria related pathway rather than the nuclear DNA mode of action similar to cisplatin, as would have been presumed due the presence of DNA intercalating ligands.

In summary, these promising findings provide great encouragement to pursue the investigations toward the use of inert Ru complexes in anticancer research.

EXPERIMENTAL SECTION

Materials. Ruthenium trichloride hydrate (Pressure Chemicals) and other chemicals were either of reagent or analytical grade and used as purchased from commercial sources. Analytical grade solvents were degassed by purging with dry, oxygen-free nitrogen for at least 30 min before use if necessary. Acetonitrile was dried by standing over calcium hydride overnight. Deionized water was used for all reactions in aqueous solution. All reagents and solvents were of HPLC grade, purchased from Acros (Geel, Belgium), Aldrich/Sigma/Fluka (Deisenhofen, Germany), Merck (Darmstadt, Germany) and IRIS Biotech (Marktredwitz, Germany) and used without further purification. $[\text{Ru}(\text{Cp}^*\text{H})(\text{CO})_2\text{Cl}_2]$,⁴⁴ $[\text{Ru}(\text{Cp}^*\text{H}-\text{NH}-\text{Hex}-\text{COOH})(\text{CO})_2\text{Cl}_2]$,⁴⁵ **1**⁴⁴ and **4**⁴⁵ were synthesized according to the literature procedures. All the characterization data was in agreement with literature reports.^{44,45}

Instrumentation and Methods. A vacuum line and Schlenk glassware were employed when reactions had to be carried out under an atmosphere of dry, oxygen-free nitrogen and assemblies were protected from light if necessary by wrapping them with aluminum foil. ¹H and ¹³C NMR spectra were measured on Bruker AC200, AM300 or DRX 400 spectrometers using the signal of the deuterated solvent as an internal standard.⁸⁹ The chemical shifts δ are reported in parts per million (ppm) relative to tetramethylsilane (TMS) or signals from the residual protons of deuterated solvents. Coupling constants *J* are given in hertz (Hz). The abbreviations for the peak multiplicities are as follows: s (singlet), d (doublet), t (triplet) and m (multiplet). ESI mass spectrometry was performed using a Bruker Esquire 6000 or a Micromass Platform II mass spectrometer fitted with an ESI source (capillary voltage was 3.5 eV and the cone voltage 35 V). In the assignment of the mass spectra, the most intense peak is listed. High-resolution accurate mass spectra were recorded with a Bruker BioApex II 47e FT-ICR MS fitted with an Analytica Electrospray Source. Samples were introduced by a syringe pump at a rate of 1 $\mu\text{L min}^{-1}$ and the capillary voltage was at 200 V. Infrared spectra were recorded on a Perkin-Elmer 1600 Series FTIR spectrometer in the range 4000–500 cm^{-1} with a resolution of $\pm 4.0 \text{ cm}^{-1}$. Samples were measured as KBr disks or neat as indicated. Microanalysis of inorganic compounds was

carried out at Campbell Microanalytical Laboratory, University of Otago, New Zealand. UV/vis spectra were recorded in 1 cm quartz cuvettes using Varian Cary Bio 300 or 5G spectrophotometers. Emission spectra were obtained following excitation at 450 nm on a Fluoromax-4 spectrofluorometer (Horiba Jobin Yvon, Inc., France) and were corrected for instrumental response using manufacturer provided correction factors. The excitation and emission slit width were set to 3.0 and 2.5 nm, respectively, for recording the emission spectra of the complexes. Emission spectra for the DNA binding evaluations were obtained following excitation at 440 nm on a Perkin-Elmer Luminescence spectrometer LS 50 B and were corrected for instrumental response using manufacturer provided correction factors. The excitation and emission slit width were set to 5.0 and 10.0 nm, respectively. Thin layer chromatography (TLC) was performed using silica gel 60 F-254 (Merck) plates with detection of spots being achieved by exposure to iodine or UV light or by using ninhydrin stain. Column chromatography was done using Silica gel 60 (0.040–0.063 mm mesh, Merck) or activated neutral alumina (Brockmann I, Sigma-Aldrich). Eluent mixtures are expressed as volume to volume (v/v) ratios.

Electrochemical Measurements. Cyclic voltammetry measurements were performed at $(20 \pm 2)^\circ\text{C}$ in acetonitrile solutions containing 0.1 M $n\text{Bu}_4\text{NPF}_6$ as the supporting electrolyte, over the scan rate range of 100–1000 mV s^{-1} using a BAS 100B (Bioanalytical Systems) electrochemical workstation. Solutions used in electrochemical measurements were deoxygenated by purging with high purity nitrogen for at least 10 min before commencing the experiments. A conventional three electrode cell was employed which comprised a glassy carbon working electrode (area = 0.0079 cm^2), a large surface area Pt counter electrode and an Ag/Ag^+ (0.1 M AgNO_3 in CH_3CN) reference electrode. The potential of the Ag/Ag^+ reference electrode was frequently calibrated against that of ferrocene/ferrocinium ($\text{Fc}^{0/+}$) redox couple under the same conditions used for voltammetric measurements with the Ru(II) complexes. The working electrode was polished with an aqueous slurry of aluminum oxide (0.3 μm), then rinsed with acetone and dried before each voltammetric experiment.

Synthesis and Characterization. $[\text{Ru}(\text{bipy})_2(\text{Cp}^{\text{NH-Hex-COOH}})](\text{PF}_6)_2 \cdot 4\text{H}_2\text{O}$ (**2**). Complex **2** was obtained as an orange solid following the same method as for **4**,⁴⁵ using 2,2'-bipyridine (bipy) (0.780 g, 5.00 mmol), trimethylamine-*N*-oxide dihydrate (1.00 g, 9.00 mmol), and $[\text{Ru}^{\text{II}}(\text{Cp}^{\text{NH-Hex-COOH}})(\text{CO})_2\text{Cl}_2]$ (1.10 g, 2.00 mmol) in 20 mL of deoxygenated 2-methoxyethanol. Yield: 1.50 g (75%). Crystals of the perchlorate salt of **2**, $[\text{Ru}(\text{bipy})_2(\text{Cp}^{\text{NH-Hex-COOH}})](\text{ClO}_4)_2 \cdot 2\text{H}_2\text{O}$, suitable for X-ray structure determination were obtained by slow evaporation of a solution prepared by dissolving a sample of the PF_6^- salt in an acetone/water mixture and then adding aqueous NaClO_4 solution (1 M). Anal. Calcd for $\text{C}_{36}\text{H}_{42}\text{F}_{12}\text{N}_8\text{O}_7\text{P}_2\text{Ru}$ (%): C, 39.68; H, 3.88; N, 10.28. Found: C, 39.81; H, 3.93; N, 10.29. IR (KBr): ν 3103 (C–H_{arom}), 2929 (C–H_{aliph}), 2864 (C–H_{aliph}), 1676 (C=O), 1533, 1438, 1413, 1243, 1162, 1020, 841, 762, 731 cm^{-1} . ^1H NMR (400 MHz, $\text{DMSO}-d_6$): δ 9.55–9.52 (m, 1H, aromatic cpp), 9.32 (d, $^3J = 7.5$ Hz, 1H, aromatic cpp), 8.82–8.79 (m, 4H, aromatic bpy), 8.28–8.24 (m, 2H, aromatic bpy), 8.20–8.14 (m, 4H, aromatic cpp and bpy), 8.05 (d, $^3J = 5.1$ Hz, 1H, –NHCO–cpp), 7.95 (d, $^3J = 5.9$ Hz, 1H, aromatic cpp), 7.78–7.73 (m, 2H, aromatic bpy), 7.71–7.65 (m, 3H, aromatic bpy), 7.56–7.51 (m, 3H, aromatic bpy), 7.49–7.46 (m, 1H, aromatic cpp), 2.21 (t, $^3J = 7.2$ Hz, 2H, –CH₂CH₂COOH), 1.63–1.51 (m, 4H, alkyl CH₂), 1.38–1.30 (m, 2H, –NH(CH₂)₂CH₂(CH₂)₂COOH) ppm. Two proton signals are masked by residual water from $\text{DMSO}-d_6$. MS (ESI⁺): m/z 364.1 $[\text{M} - 2\text{PF}_6]^{2+}$, 873.1 $[\text{M} - \text{PF}_6]^+$. HR-ESI mass spectrum ($\text{CH}_3\text{CN}/\text{MeOH}$ 1:4): found 364.0902; calcd for $[\text{C}_{36}\text{H}_{34}\text{N}_8\text{O}_3\text{Ru}]^+/z$ 364.0899. $\epsilon_{440} = 12\,900 \text{ M}^{-1}\text{cm}^{-1}$ (H_2O in 0.2% DMSO).

$[\text{Ru}(\text{dppz})_2(\text{Cp}^{\text{NH}})](\text{PF}_6)_2 \cdot 4\text{H}_2\text{O}$ (**3**). Complex **3** was prepared in a similar manner to **2**, using dipyrrido[3,2-*a*:2',3'-*c*]phenazine (dppz) (0.212 g, 0.752 mmol), trimethylamine-*N*-oxide dihydrate (0.150 g, 1.35 mmol), and $[\text{Ru}^{\text{II}}(\text{Cp}^{\text{NH}})(\text{CO})_2(\text{Cl})_2]$ (0.129 g, 0.301 mmol) in 12 mL of 2-methoxyethanol. The crude product was purified by column chromatography on neutral alumina, gradually changing the

eluent from $\text{CH}_3\text{CN}/\text{H}_2\text{O}/\text{sat. KNO}_3$ (16:3:1) to $\text{CH}_3\text{CN}/\text{H}_2\text{O}/\text{sat. KNO}_3$ (10:3:1). The dark orange band was collected, and the solvent removed under reduced pressure. The concentrate was passed through a Sephadex LH-20 column with acetonitrile as eluent to remove inorganic salts. The intense orange band was collected, concentrated and the residue suspended in water followed by dropwise addition of HPF_6 (60%) to complete the precipitation of the product as a hexafluorophosphate salt. The precipitate was collected by filtration, washed with hot toluene and dried *in vacuo* to obtain **3** as an orange solid. Yield: 0.228 g (66%). Anal. Calcd for $\text{C}_{46}\text{H}_{35}\text{F}_{12}\text{N}_{11}\text{O}_6\text{P}_2\text{Ru}$ (%): C, 44.96; H, 2.87; N, 12.54. Found: C, 45.11; H, 2.98; N, 12.58. IR (KBr): ν 1717 (C=O), 1636, 1420, 1357, 1234, 1079, 844, 763, 729 cm^{-1} . ^1H NMR (400 MHz, $\text{DMSO}-d_6$): δ 9.66–9.64 (m, 2H, aromatic dppz), 9.57–9.54 (m, 2H, aromatic dppz), 8.94 (d, $^3J = 7.8$ Hz, 1H, aromatic cpp), 8.63–8.61 (m, 1H, aromatic cpp), 8.52–8.46 (m, 4H, aromatic dppz), 8.35–8.33 (m, 1H, aromatic cpp), 8.29–8.25 (m, 2H, aromatic dppz), 8.23–8.16 (m, 5H, aromatic dppz), 8.12–8.06 (m, 3H, aromatic cpp and dppz), 7.91–7.85 (m, 3H, aromatic cpp and dppz), 7.60–7.54 (m, 2H, aromatic dppz) ppm. MS (ESI⁺): m/z 433.3 $[\text{M} - 2\text{PF}_6]^{2+}$. HR-ESI mass spectrum ($\text{CH}_3\text{CN}/\text{MeOH}$ 1:4): found 433.5704; calcd for $[\text{C}_{46}\text{H}_{27}\text{N}_{11}\text{O}_2\text{Ru}]^+/z$ 433.5696. $\epsilon_{440} = 19\,650 \text{ M}^{-1}\text{cm}^{-1}$ (H_2O in 0.2% DMSO).

Distribution Coefficients. The distribution coefficient of each complex, defined as

$$\log D_{o/w} = \log \left(\frac{[\text{solute}]_{\text{octanol}}}{[\text{solute}]_{\text{water}}^{\text{ionized}} + [\text{solute}]_{\text{water}}^{\text{neutral}}} \right)$$

was experimentally determined by using the “shake-flask” method. Briefly, each complex was dissolved in a 10 mM phosphate buffer (pH 7.01), previously saturated with octanol, to give about 1 mL of a solution with a concentration reported in Table 4 for each complex.

Table 4. Extinction Coefficients (ϵ) of Ru(II) Complexes 1–4

| complex | λ_{max} [MLCT] (nm) | ϵ_{molar} ($\text{M}^{-1}\text{cm}^{-1}$) | |
|---------|------------------------------------|---|---|
| | | phosphate buffer (10 mM, pH 7.01) ^a | H_2O (0.2% DMSO) ^b |
| 1 | 444 | 12500 | 13400 |
| 2 | 440 | 12300 | 12900 |
| 3 | 451 | 17400 | 14500 |
| 4 | 451 | 17600 | 18200 |

^a[1] = 50 μM , [2] = 50 μM , [3] = 42 μM and [4] = 37 μM .
^b[complex] = 10 μM .

The same volume of octanol (previously saturated with 10 mM phosphate buffer) was then added and the solution was shaken 100 times and equilibrated for 4.5 h. The concentration of the complex in the aqueous phase was then evaluated by UV–vis spectroscopy, using extinction coefficients for PBS solutions of the complexes (Table 4). The evaluation on each complex was repeated 3 times.

DNA Binding (UV–visible and Fluorescence Experiments). DNA and Ru complexes concentrations were evaluated by spectroscopy, using the extinction coefficients presented in Table 4.

The absorption titrations were performed at room temperature in 10 mM phosphate buffer with 50 mM NaCl (pH 7.01). For every sample, the Ru complex concentration was constant, between 3 μM and 20 μM , depending on the compound, and a concentrated solution of CT DNA (type I, fibers) was added ($\epsilon_{260, \text{CTDNA}} = 6600 \text{ M}^{-1}\text{cm}^{-1}$ per nucleotide). A reference cell loaded with buffer was necessary, in which the DNA was added each time, to minimize the changes due to the DNA in absorption at 260 nm. After every addition, samples were incubated at room temperature for 10 min, and then the UV–visible spectra were recorded. Additions of DNA were carried on until no further changes in spectra were observed.

Fluorescent DNA titrations were performed in the same way, by using Ru complex solution between 3 and 27 μM , depending on the

complex, in the same buffer and by adding DNA until no more changes were observed. In these cases, no reference cell was necessary.

DNA binding constant (K_b) was determined by fitting the titration data to the McGhee-Von Hippel equation, as previously reported.^{81,82}

$$(\epsilon_a - \epsilon_f)/(\epsilon_b - \epsilon_f) = (b - (b^2 - 2K_b^2C[\text{DNA}]/s))^{1/2}/2K_bC$$

$$b = 1 + K_bC + K_b[\text{DNA}]/2s$$

where [DNA] is the concentration of CT-DNA in nucleotides, ϵ_a is the apparent extinction coefficient of Ru complexes at a given DNA concentration, ϵ_f is the extinction coefficient of Ru complexes in absence of DNA, ϵ_b is the extinction coefficient of Ru complexes when completely bound to DNA, C is the total Ru complex concentration, and s is the binding site size in base pairs. From plots of $(\epsilon_a - \epsilon_f)/(\epsilon_b - \epsilon_f)$ versus [DNA], K_b values were calculated by fitting the curves with OriginLab 8.6.

DNA binding constants from emission data were determined by fitting the data with the same equation, but using I_a instead of ϵ_a , as the luminescence intensity of ruthenium complexes at a given DNA concentration, and I_f and I_b (instead of ϵ_f and ϵ_b), as the luminescence intensity of complexes in their free and completely bound forms, respectively.

DNA Binding (Gel Experiments). To test the DNA binding ability of metal complexes, 0.5 μg of 1 kb DNA ladder (New England BioLabs) was resolved on multiple lanes of a 1% agarose gel. Individual lanes were excised and incubated with 2.5 μM ruthenium complex solutions. As positive control, a lane of the agarose gel was stained with ethidium bromide (EtBr). The reconstituted gel was analyzed using an Alpha Innotech Imaging system with the EtBr colorimetric filter (365 nm).

Protein Binding. To test the protein binding ability of metal complexes, 3 μg of Broad Range Molecular Weight Markers (Bio-Rad) were resolved on multiple lanes of an 8% SDS-gel. Individual lanes were excised, fixed with 30% ethanol/10% acetic acid and incubated with 2.5 μM ruthenium complex solutions. Coomassie blue staining was taken as a positive control. The reconstituted gel was analyzed using an Alpha Innotech Imaging system using visible light as illumination source.

Stability of 3 in Human Plasma. These experiments were performed following a procedure recently described by our group.⁶⁵ The human plasma was provided by the Blutspendezentrum, Zurich, Switzerland. Diazepam (internal standard) was obtained from Sigma-Aldrich. Stock solutions of 3 (20 mM) and diazepam (800 μM) were prepared in DMSO. For a typical experiment, an aliquot of the respective stock solutions and DMSO were then added to the plasma solution (975 μL) to a total volume of 1000 μL and final concentrations of 20 μM for 3 and 10 μM of diazepam. The resulting plasma solution was incubated for 72 h at 37 $^\circ\text{C}$ with continuous and gentle shaking (ca. 300 rpm). The reaction was stopped by addition of 2 mL of methanol, and the mixture was centrifuged for 45 min at 650g at 4 $^\circ\text{C}$. The methanolic solution was evaporated and the residue was suspended in 200 μL of 1:1 (v/v) acetonitrile/ H_2O solution. The suspension was filtered and analyzed using LC-MS. A total of 40 μL of the solution was injected into the HPLC (Acquity Ultra Performance LC, Waters) that was connected to a mass spectrometer (Bruker Esquire 6000) operated in ESI mode. The Nucleosil 100-5 C18 (250 \times 3 mm) reverse phase column was used with a flow rate of 0.5 mL min^{-1} and UV-absorption was measured at 300 nm. The runs were performed with a linear gradient of A (acetonitrile) (Sigma-Aldrich HPLC-grade) and B (distilled water containing 0.02% TFA and 0.05% HCOOH): $t = 0\text{--}3$ min, 20% A; $t = 7$ min, 50% A; $t = 20$ min, 90% A; $t = 23$ min, 100% A; $t = 25$ min, 100% A; $t = 28$ min, 20% A.

Cell Culture. Human cervical carcinoma (HeLa) cells were cultured in DMEM (Gibco) supplemented with 5% fetal calf serum (FCS, Gibco), 100 U/mL penicillin, 100 $\mu\text{g}/\text{mL}$ streptomycin at 37 $^\circ\text{C}$ and 5% CO_2 . The human osteosarcoma cell line U2OS was maintained in DMEM (Gibco) supplemented with 10% FCS (Gibco), penicillin (100 U/mL), and streptomycin (100 $\mu\text{g}/\text{mL}$). The human breast carcinoma MCF7 cell line was cultured in MEM medium

(Gibco) supplemented with 10% FCS (Gibco), 200 mM L-glutamine, penicillin (100 U/mL), and streptomycin (100 $\mu\text{g}/\text{mL}$). The human ovarian carcinoma A2780 cell line and a cisplatin-resistant subline CP70 were cultured in RPMI-1640 medium (Gibco) supplemented with 10% FCS (Gibco), penicillin (100 U/mL), and streptomycin (100 $\mu\text{g}/\text{mL}$). The normal human fetal lung fibroblast MRC-5 cell line was maintained in F-10 medium (Gibco) supplemented with 10% FCS (Gibco), penicillin (100 U/mL), and streptomycin (100 $\mu\text{g}/\text{mL}$).

In Vitro Fluorescence Evaluation. Cellular localization of fluorescent ruthenium complexes was assessed by fluorescence microscopy. HeLa cells were grown on 35 mm Cellview glass bottom dishes (Greiner) or on 18 mm Menzel-gläser coverslips at a density of 1×10^5 cells/mL and incubated for 2 h with ruthenium complexes at their IC_{50} or at 100 μM for nontoxic complexes. Cells were fixed in 4% formaldehyde solution (10% formaldehyde in 90% PBS) and either mounted on slides for viewing by confocal microscopy or kept in water for imaging on an Olympus IX 81 motorized inverted microscope (Olympus, Hamburg, Germany), using 10 \times dry and 60 \times oil-immersion lenses and digital camera. Alternatively, fixed cells were viewed on a CLSM Leica SP5 microscope. The ruthenium complexes were visualized using the Cy3 filter set of the Olympus microscope (ex., 550 nm; em., 570 nm) or using the red wavelength selection (ex, 458 nm; em, 600–650 nm) on the CLSM Leica SP5 microscope.

Mitochondrial Staining. Colocalization of ruthenium complex 3 with mitochondria was examined by means of Mitotracker green FM (Molecular Probes), a mitochondria-specific dye.⁴¹ Briefly, a 1 mM Mitotracker Green FM stock solution made in DMSO was diluted to 10 μM working concentration in cell medium (DMEM, 5% FCS). Staining of mitochondria was accomplished by adding a 50 nM final concentration of Mitotracker Green FM to the culture medium for the last 45 min of ruthenium complex incubation. The medium was removed and cells were fixed in 4% formaldehyde solution before being mounted on slides for viewing by confocal microscope.

Cytotoxicity Studies. Cytotoxicity studies were performed on six different cell lines, namely, HeLa, MCF7, U2OS, A2780, CP-70 and MRC-5, by a fluorometric cell viability assay using Resazurin (Promocell GmbH). Briefly, one day before treatment, cells were plated in triplicates in 96-well plates at a density of 4×10^3 cells/well in 100 μL . Upon treating cells with increasing concentrations of the ruthenium complexes for 48 h, the medium was removed, and 100 μL of complete medium containing resazurin (0.2 mg/mL final concentration) was added. After 4 h of incubation at 37 $^\circ\text{C}$, the fluorescence of the highly red fluorescent resorufin product was quantified at 590 nm emission with 540 nm excitation wavelength in a SpectraMax M5 microplate Reader.

Flow Cytometry. HeLa cells suspensions were washed twice in 1 \times PBS and centrifuged at 130g for 6 min to remove the medium and the metal complex. The cellular uptake of ruthenium complex was detected in the PE-Texas Red channel (excitation at 488 nm; emission at 575/25 nm). JC-1 monomers used in determination of the mitochondrial membrane potential health condition as well as annexin V-FITC conjugate used in the detection of apoptotic cells were detected in the FITC channel, whereas JC-1 aggregates were detected in the APC channel. A total of 15 000 cells were collected for each sample by the flow cytometer CyAn ADP 9 and analyzed with Summit 4.3 software. Nonviable cells were excluded from the analysis. Data are represented as mean \pm SEM.

Uptake Studies. To determine the cellular uptake efficiency of ruthenium complex 3, flow cytometric analysis was performed. To this end, 3×10^5 HeLa cells were seeded in 6 cm dishes one day before treatment and incubated at 4, 23, and 37 $^\circ\text{C}$ and 5% CO_2 for 6 h with 20 μM of 3. The cells were treated with trypsin, centrifuged, washed twice in 1 \times PBS and finally resuspended in 1 tmePBS prior to flow cytometric analysis.

Evaluation of Mitochondrial Membrane Potential ($\Delta\Psi\text{m}$). The mitochondrial membrane potential was measured by the JC-1 (5,5',6,6'-tetrachloro-1,1',3,3'-tetraethylbenzimidazolylcarbocyanine iodide) (Sigma-Aldrich). HeLa cells were seeded in 6-well plates at a density of 4×10^5 cells one day before treatment and incubated for 2, 24, and 48 h with 20 μM 3 at either 4, 23, or 37 $^\circ\text{C}$. Following this,

cells were then treated with trypsin and resuspended in 5 mL of complete medium. The cell suspension was then stained according to the manufacturer's instructions.

Intracellular ROS Measurement. The production of intracellular ROS was detected by 2',7'-dichlorofluorescein diacetate (H₂DCF-DA, Sigma-Aldrich), a cell-permeable nonfluorescent probe which is de-esterified in cell and upon oxidation turns to highly fluorescent 2',7'-dichlorofluorescein. HeLa cells were seeded in white 96-well plates at a density of 8×10^3 cells one day before treatment. The medium was removed and H₂DCF-DA (10 μ M) was added to cells for 30 min at 37 °C in the dark. The cells were subsequently washed in serum-free medium and treated for 30 min, 1 h, 2 h, or 6 h with **3**, in presence or absence of 10 mM NAC, an antioxidant. Fluorescence was quantified at 530 nm emission with 488 nm excitation wavelength in a SpectraMax M5 microplate Reader.

Apoptosis Detection. Apoptosis was detected by means of YO-PRO (Molecular Probes) staining, a nucleic acid dye permeating exclusively apoptotic cells. HeLa cells were seeded in 96-well plates at a density of 5×10^3 cells one day before treatment. The medium was replaced and cells were treated for 2, 24, 48, or 72 h with **3** (20 μ M). YO-PRO (2.5 μ M final concentration in 20 mM Na-citrate pH 4.0, 26.8 mM NaCl) was added to the culture medium for 10 min at 25 °C in the dark. Fluorescence was quantified at 530 nm emission with 485 nm excitation wavelength in a SpectraMax M5 microplate Reader. Finally, cells were lysed in 25 μ L of lysis buffer (0.1% NP40, 5 mM EDTA, 5 mM EGTA) for 30 min at 25 °C in the dark and fluorescence was quantified again. The ratio between the fluorescence measured before and after lysis equals the percentage of apoptotic cells in the population examined.

Apoptosis was also detected by means of annexin V-FITC conjugate purchased from BD Pharmingen (BD Bioscience), which has a high affinity binding for the membrane phospholipid phosphatidylserine, translocated from the inner to the outer leaflet of the plasma membrane during apoptosis. HeLa cells were seeded in 6 cm dishes at a density of 4×10^5 cells one day before treatment. The medium was replaced and cells were treated for 2, 24, 48, or 72 h with **3** (20 μ M). Cells were then stained with annexin V-FITC according to the manufacturer's instructions.

Caspase 3/7 Assay. Caspases 3/7 activity was assessed using the Caspase-Glo 3/7 assay kit (Promega). HeLa cells were seeded in white 96-well plates at a density of 8×10^3 cells one day before treatment. Cells were treated with **3** (20 μ M) for 24 h or with 150 nM staurosporin for 6 h at 37 °C. Caspase 3/7 activity was detected according to the manufacturer's instructions. Luminescence in RLU was quantified in a SpectraMax M5 microplate Reader.

Mitochondria Isolation from HeLa Cells. Mitochondria were isolated by means of the Mitochondria isolation kit (Sigma Aldrich). HeLa cells were cultured in 175 cm² flask at a density of 13×10^6 cells and treated with 50 μ M of **3**. Mitochondria were then isolated from whole cell extract according to the manufacturer's instructions. Before the isolation procedure, an aliquot was removed to determine the total cellular ruthenium concentration. Mitochondria, as well as cell pellets, were then lyophilized prior Atomic Absorption measurements.

HR-CS AAS Measurements. For metal quantification, the lyophilized samples were resuspended in 100 μ L of deionized water and 100 μ L of storage buffer (1:5) for mitochondria pellets. An aliquot of 10 μ L was then removed to quantify the protein concentration of the samples by Bradford method.⁶⁴ A contrAA 700 high-resolution continuum source atomic absorption spectrometer (AnalytikJena AG) was used for the ruthenium quantification at a wavelength of 349.900 nm. Aqueous standard samples of **3** were used for calibration purposes. To 90 μ L of all probes and standards each 9 μ L Triton X-100 (1%) and 9 μ L hydrochloric acid (18%) were added. Samples were injected at a volume of 25 μ L into coated standard graphite tubes ("AAS IC-Standardrohr, beschichtet", AnalytikJena AG). A furnace program as described in the literature was used.³⁰ During the temperature program, the graphite tube was purged with a constant argon gas flow, which was only halted during the zeroing and atomization steps. The mean integrated absorbances of double injections were used throughout the study. The results are expressed as nmol ruthenium

per milligram of protein. A percentage value of **3** accumulated in mitochondria compared to the total cellular ruthenium concentration was also calculated.

X-ray Crystallography. Intensity data for red crystals of **1** (0.20 \times 0.20 \times 0.05 mm) and **2** (0.38 \times 0.10 \times 0.05 mm) were measured at 173 K on a Bruker Apex II CCD fitted with graphite monochromated Mo K α radiation (0.71073 Å). The data were collected to a maximum 2 θ value of 50° and processed using the Bruker Apex II software package. Crystal parameters and details of the data collection are summarized in Table S4 in the Supporting Information. Each structure was solved by direct methods and expanded using standard Fourier routines in the SHELX-97.^{90,91} All hydrogen atoms were placed in idealized positions, except for the hydrogen on the oxygen atom of the carboxylic group and the nitrogen atom (in **2**) which were located on the Fourier difference map and refined with restrained O–H and N–H distances. The isotropic thermal parameters for O–H and N–H hydrogen atoms were fixed at 1.2 times that of the respective oxygen or nitrogen atom. A PF₆[−] counteranion in **1** and ClO₄[−] counteranion in **2** were found disordered and refined anisotropically using part command. The hydrogen atoms associated with the water molecules of crystallization could not be located on the Fourier Difference map. All non-hydrogen atoms were refined anisotropically.

Abbreviations. AAS, atomic absorption spectrometry; bipy, 2,2'-bipyridine; Boc, *tert*-butoxycarbonyl; CppH, 2-(2'-pyridyl)pyrimidine-4-carboxylic acid; Cpp-NH-Hex-COOH, 6-(2-(pyridin-2-yl)-pyrimidine-4-carboxamido)hexanoic acid; CT-DNA, calf-thymus DNA; dppz, dipyrido[3,2-*a*:2',3'-*c*]phenazine; DIPEA, diisopropylethylamine; ESI-MS, electrospray ionisation mass spectrometry; Fmoc, fluorenylmethoxycarbonyl; Gly, glycine; HR-CS AAS, high-resolution continuum source atomic absorption spectrometry; KP1019, *trans*-[tetrachlorobis(1*H*-indazole)ruthenate(III)]; MALDI-TOF, matrix assisted laser/desorption ionization–time of flight; NAC, *N*-acetylcysteine; NAMI-A, *trans*-[tetrachloro(dimethylsulfoxide)-(1*H*-imidazole)ruthenate(III)].

■ ASSOCIATED CONTENT

● Supporting Information

¹H NMR spectra of **2** and **3** (Figures S1–S2), absorption and emission spectra of **1–4** (Figures S3–S4), thermal ellipsoid plots of **1** and **2** (Figures S5–S6), molecular packing of **2** (Figure S7), selected bond lengths and angles for **1** and **2** (Table S1), plots of the Resazurin assays of **3**, cisplatin and dequalinium chloride hydrate (Figures S8–S10), fluorescence confocal microscopy images of **1–4** in HeLa cells (Figure S11), UV traces (300 nm) of the LC–MS analysis of **3** in human plasma at $t = 0$ and 72 h (Figure S12), ratios of peak areas of **3**/Diazepam in human plasma at $t = 0$ and 72 h (Table S2), flow cytometry dot plots of the uptake of **3** (Figure S13), effect of temperature on the uptake of **3** (Figure S14), cyclic voltammetric data of **2–4** (Table S3), cyclic voltammograms of **2–4** (Figures S15–S18), CT-DNA titration of **1–4** (Figures S19–S24), gels for DNA and protein binding of **1–4** (Figures S25–S26), annexin-V activity measurements of **3** (Figure S27), caspase 3/7 activity measurements of **3** (Figure S28), ROS production measurements of **3** (Figure S29), flow cytometry dot plots of MMP of **3** in HeLa cells (Figure S30), effect of **3** with temperature on mitochondrial potential of HeLa cells (Figure S31), crystallography collection and refinement data of **1** and **2** (Table S4). X-ray crystallographic files for **1** and **2** in CIF format. Video of the colocalization studies of **3** in avi format. This material is available free of charge via the Internet at <http://pubs.acs.org>.

■ AUTHOR INFORMATION

Corresponding Author

leone.spiccia@monash.edu; sferrari@imcr.uzh.ch; gilles.gasser@aci.uzh.ch

Notes

The authors declare no competing financial interest.

■ ACKNOWLEDGMENTS

This work was financially supported by the Swiss National Science Foundation (SNSF Professorship to G.G. and Research Grants to G.G. and S.F.), the University of Zurich (G.G. and S.F.), the Stiftung für Wissenschaftliche Forschung of the University of Zurich (S.F.), the Stiftung zur Krebsbekämpfung (S.F.), the Huggenberger-Bischoff Stiftung (S.F.), the University of Zurich Priority Program (S.F.), the Fonds der Chemischen Industrie (I.O.), and the Australian Research Council through the Australian Centre of Excellence for Electromaterials Science (L.S.). T.J. is a recipient of Monash Graduate Scholarship, Monash International Postgraduate Research Scholarship and Postgraduate Publication Award. The authors thank Prof. Alan M. Bond and Dr. Malay Patra for helpful discussions and Dr. Urs Ziegler (University of Zurich, Center for Microscopy and Image Analysis) for guidance in the optimization of cell imaging.

■ REFERENCES

- (1) Rosenberg, B.; VanCamp, L.; Krigas, T. *Nature* **1965**, *222*, 385–386.
- (2) Fricker, S. P. *Dalton Trans.* **2007**, 4903–4917 and references therein.
- (3) Lippert, B. *Cisplatin, Chemistry and Biochemistry of a Leading Anticancer Drug*; Verlag Helvetica Chimica Acta: Zürich, 1999.
- (4) Dhar, S.; Lippard, S. J. In *Bioinorganic Medicinal Chemistry*; Alessio, E., Ed.; Wiley-VCH: Weinheim, 2011; pp 351–382.
- (5) Dabrowiak, J. C. *Metals in Medicine*; John Wiley & Sons Ltd: Chichester, 2009.
- (6) *Bioinorganic Medicinal Chemistry*; Alessio, E., Ed.; Wiley-VCH Verlag: Weinheim, 2011.
- (7) Sessler, J. L.; Doctrow, S. R.; McMurry, T. J.; Lippard, S. J. *Medicinal Inorganic Chemistry*; American Chemical Society: Washington, D.C, 2005; Vol. 903.
- (8) Bratsos, I.; Gianferrara, T.; Alessio, E.; Hartinger, C. G.; Jakupec, M. A.; Keppler, B. K. In *Bioinorganic Medicinal Chemistry*; Alessio, E., Ed.; Wiley-VCH: Weinheim, 2011; pp 151–174.
- (9) Süß-Fink, G. *Dalton Trans.* **2010**, 39, 1673–1688 and references therein.
- (10) Dyson, P. J.; Sava, G. *Dalton Trans.* **2006**, 1929–1933 and references therein.
- (11) Dougan, S. J.; Sadler, P. J. *Chimia* **2007**, *61*, 704–715.
- (12) Melchart, M.; Sadler, P. J. In *Bioorganometallics*; Jaouen, G., Ed.; Wiley-VCH: Weinheim, 2006; pp 39–64.
- (13) Peacock, A. F. A.; Sadler, P. J. *Chem. Asian J.* **2008**, *3*, 1890–1899.
- (14) Gasser, G.; Ott, I.; Metzler-Nolte, N. *J. Med. Chem.* **2011**, *54*, 3–25.
- (15) Sava, G.; Bergamo, A.; Dyson, P. J. *Dalton Trans.* **2011**, *40*, 9069–9075.
- (16) Smith, G. S.; Therrien, B. *Dalton Trans.* **2011**, *40*, 10793–10800.
- (17) Gianferrara, T.; Bratsos, I.; Alessio, E. *Dalton Trans.* **2009**, 7588–7598.
- (18) Gasser, G.; Metzler-Nolte, N. *Curr. Opin. Chem. Biol.* **2012**, *16*, 84–91.
- (19) Sava, G.; Zorzet, S.; Turrin, C.; Vita, F.; Soranzo, M. R.; Zabucchi, G.; Cocchietto, M.; Bergamo, A.; Di Giovine, S.; Pezzoni, G.; Sartor, L.; Garbisa, S. *Clin. Cancer Res.* **2003**, *9*, 1898–1905.
- (20) Bergamo, A.; Sava, G. *Dalton Trans.* **2011**, *40*, 7817–7823.
- (21) Hartinger, C. G.; Jakupec, M. A.; Zorbas-Seifried, S.; Groessl, M.; Egger, A.; Berger, W.; Zorbas, H.; Dyson, P. J.; Keppler, B. K. *Chem. Biodiversity* **2005**, *5*, 2140–2154 and references therein.
- (22) Bratsos, I.; Jedner, S.; Gianferrara, T.; Alessio, E. *Chimia* **2007**, *61*, 692–697.
- (23) Hartinger, C. G.; Jakupec, M. A.; Zorbas-Seifried, S.; Groessl, M.; Egger, A.; Berger, W.; Zorbas, H.; Dyson, P. J.; Keppler, B. K. *Chem. Biodiversity* **2008**, *5*, 2140–2154 and references therein.
- (24) Sava, G.; Alessio, E.; Bergamo, A.; Mestroni, G. In *Metallopharmaceuticals*; Clarke, M. J., Sadler, P. J., Eds.; Springer: Berlin, 1999; Vol. 1, pp 143–169.
- (25) Mulcahy, S. P.; Meggers, E. In *Medicinal Organometallic Chemistry*; Jaouen, G., Metzler-Nolte, N., Eds.; Springer-Verlag: Heidelberg, 2010; Vol. 32, pp 141–153.
- (26) Meggers, E. *Chem. Commun.* **2009**, 1001–1010 and references therein.
- (27) Gasser, G.; Metzler-Nolte, N. In *Bioinorganic Medicinal Chemistry*; Alessio, E., Ed.; Wiley-VCH Verlag: Weinheim, 2011; pp 351–382.
- (28) Gill, M. R.; Thomas, J. A. *Chem. Soc. Rev.* **2012**, *41*, 3179–3192.
- (29) Kilah, N. L.; Meggers, E. *Aust. J. Chem.* **2012**, *65*, 1325–1332 and references therein.
- (30) Schaefer, S.; Ott, I.; Gust, R.; Sheldrick, W. S. *Eur. J. Inorg. Chem.* **2007**, 3034–3046.
- (31) Gill, M. R.; Derrat, H.; Smythe, C. G. W.; Battaglia, G.; Thomas, J. A. *ChemBioChem* **2011**, *12*, 877–880.
- (32) Tan, C.; Wu, S.; Lai, S.; Wang, M.; Chen, Y.; Zhou, L.; Zhu, Y.; Lian, W.; Peng, W.; Ji, L.; Xu, A. *Dalton Trans.* **2011**, *40*, 8611–8621.
- (33) Tan, C.; Lai, S.; Wu, S.; Hu, S.; Zhou, L.; Chen, Y.; Wang, M.; Zhu, Y.; Lian, W.; Peng, W.; Ji, L.; Xu, A. *J. Med. Chem.* **2010**, *53*, 7613–7624.
- (34) Liu, J.; Zheng, W.; Shi, S.; Tan, C.; Chen, J.; K., Z.; Ji, L. *J. Inorg. Biochem.* **2008**, *102*, 193–202.
- (35) Salassa, L. *Eur. J. Inorg. Chem.* **2011**, *32*, 4931–4947 and references therein.
- (36) Corral, E.; Hotze, A. C. G.; den Dulk, H.; Leczkowska, A.; Rodger, A.; Hannon, M. J.; Reedijk, J. *J. Biol. Inorg. Chem.* **2009**, *14*, 439–448.
- (37) Huang, H.-L.; Zheng-Zheng, Li, Z.-Z.; Liang, Z.-H.; Liu, Y.-J. *Eur. J. Inorg. Chem.* **2011**, 5538–5547.
- (38) Schatzschneider, U.; Niesel, J.; Ott, I.; Gust, R.; Alborzina, H.; Wölfl, S. *ChemMedChem* **2009**, *3*, 1104–1109.
- (39) Kou, J.-F.; Qian, C.; Wang, J.-Q.; Chen, X.; Wang, L.-L.; Chao, H.; Ji, L.-N. *J. Biol. Inorg. Chem.* **2012**, *17*, 81–96.
- (40) Chen, T.; Liu, Y.; Zheng, W.-J.; Liu, J.; Wong, Y.-S. *Inorg. Chem.* **2010**, *49*, 6366–6388.
- (41) Pisani, M. J.; Fromm, P. D.; Mulyana, Y.; Clarke, R. J.; Körner, H.; Heimann, K.; Collins, J. G.; Keene, F. R. *ChemMedChem* **2011**, *6*, 848–858.
- (42) Mulcahy, S. P.; Gründler, K.; Frias, C.; Wagner, L.; Prokop, A.; Meggers, E. *Dalton Trans.* **2010**, 39, 8177–8182.
- (43) Chen, T.; Mei, W.-J.; Wong, Y.-S.; Liu, J.; Liu, Y.; Xie, H.-S.; Zheng, W.-J. *MedChemComm* **2012**, *1*, 73–75.
- (44) Nickita, N.; Gasser, G.; Pearson, P.; Goh, L. Y.; Bond, A. M.; Deacon, G. B.; Spiccia, L. *Inorg. Chem.* **2009**, *48*, 68–81.
- (45) Joshi, T.; Barbante, G. J.; Francis, P. S.; Hogan, C. F.; Bond, A. M.; Gasser, G.; Spiccia, L. *Inorg. Chem.* **2012**, *51*, 3302–3315.
- (46) Joshi, T.; Barbante, G. J.; Francis, P. S.; Hogan, C. F.; Bond, A. M.; Spiccia, L. *Inorg. Chem.* **2011**, *50*, 12172–12183.
- (47) Joshi, T.; Gasser, G.; Martin, L. L.; Spiccia, L. *RSC Adv.* **2012**, *2*, 4703–4712.
- (48) Nickita, N.; Belousoff, Bhatt, A. I.; Bond, A. M.; Deacon, G. B.; Gasser, G.; Spiccia, L. *Inorg. Chem.* **2007**, *46*, 8638–8651.
- (49) Ahmed, S. A.; Gogal, R. M. J.; Walsh, J. E. *J. Immunol. Methods* **1994**, *170*, 211–224.
- (50) Weiss, M. J.; Wong, J. R.; Ha, C. S.; Bleday, R.; Salem, R. R.; Steele, G. D. J., Jr.; Chen, L. B. *Proc. Natl. Acad. Sci. U.S.A.* **1987**, *84*, 5444–5448.

- (51) Galeano, E.; Nieto, E.; García-Pérez, A. I.; Delgado, M. D.; Pinilla, M.; Sancho, P. *Leuk. Res.* **2005**, *29*, 1201–1211.
- (52) Siddik, Z. H. *Oncogene* **2003**, *22*, 7265–7279 and references therein.
- (53) Ke, H.; Wang, H.; Wong, W. K.; Mak, N. K.; Kwong, D. W.; Wong, K. L.; Tam, H. L. *Chem. Commun.* **2010**, *46*, 6678–6680.
- (54) Kasper, C.; Alborzina, H.; Can, S.; Kitanovic, I.; Meyer, A.; Geldmacher, Y.; Oleszak, M.; Ott, I.; Wöfl, S.; Sheldrick, W. S. *J. Inorg. Biochem.* **2012**, *106*, 126–133.
- (55) Barnard, P. J.; Wedlock, L. E.; Baker, M. V.; Berners-Price, S. J.; Joyce, D. A.; Skeleton, B. W.; Steer, J. H. *Angew. Chem., Int. Ed.* **2006**, *45*, 5966–5970.
- (56) Berners-Price, S. J. In *Bioinorganic Medicinal Chemistry*; Alessio, E., Ed.; Wiley-VCH: Weinheim, 2011; pp 197–222.
- (57) Rackham, O.; Nichols, S. J.; Leedman, P. J.; Berners-Price, S. J.; Filipovska, A. *Biochem. Pharmacol.* **2007**, *74*, 992–1002.
- (58) Barnard, P. J.; Berners-Price, S. J. *Coord. Chem. Rev.* **2007**, *251*, 1889–1902.
- (59) Rubbiani, R.; Can, S.; Kitanovic, I.; Alborzina, H.; Stefanopoulou, M.; Kokoschka, M.; Mönchgesang, S.; Sheldrick, W. S.; Wöfl, S.; Ott, I. *J. Med. Chem.* **2011**, *54*, 8646–8657.
- (60) Kirin, S. I.; Ott, I.; Gust, R.; Mier, W.; Weyhermueller, T.; Metzler-Nolte, N. *Angew. Chem., Int. Ed.* **2008**, *47*, 955–959.
- (61) Patra, M.; Gasser, G.; Pinto, A.; Merz, K.; Ott, I.; Bandow, J. E.; Metzler-Nolte, N. *ChemMedChem* **2009**, *4*, 1930–1938.
- (62) Ott, I.; Scharwitz, M.; Scheffler, H.; Sheldrick, W. S.; Gust, R. *J. Pharm. Biomed. Anal.* **2008**, *47*, 938–942.
- (63) Oehninger, L.; Stefanopoulou, M.; Alborzina, H.; Schur, J.; Ludewig, S.; Namikawa, K.; Muñoz-Castro, A.; Köster, R. W.; Baumann, K.; Wöfl, S.; Sheldrick, W. S.; Ott, I. *Dalton Trans.* **2013**, DOI: 10.1039/c2dt32319b.
- (64) Bradford, M. M. *Anal. Biochem.* **1976**, *72*, 248–254.
- (65) Patra, M.; Ingram, K.; Pierroz, V.; Ferrari, S.; Spingler, B.; Keiser, J.; Gasser, G. *J. Med. Chem.* **2012**, *55*, 8790–8798.
- (66) Puckett, C. A.; Ernst, R. J.; Barton, J. K. *Dalton Trans.* **2010**, *39*, 1159–1170.
- (67) Puckett, C. A.; Barton, J. K. *J. Am. Chem. Soc.* **2007**, *129*, 46–47.
- (68) Puckett, C. A.; Barton, J. K. *Biochemistry* **2008**, *47*, 11711–11716.
- (69) Liberman, E. A.; Topali, V. P.; Tsofina, L. M.; Jasaitis, A. A.; Skulachev, V. P. *Nature* **1969**, *222*, 1076–1078.
- (70) Johnson, L. V.; Walsh, M. L.; Chen, L. B. *Proc. Natl. Acad. Sci. U.S.A.* **1980**, *77*, 990–994.
- (71) Bard, A. J.; Faulkner, L. R. *Electrochemical Methods, Fundamentals and Application*; 2nd ed.; Brisbane: Australia, 2001.
- (72) Sevcik, A. *Collect. Czech. Chem. Commun.* **1948**, *13*, 349–377.
- (73) Randles, J. E. B. *Trans. Faraday Soc.* **1948**, *44*, 322–327.
- (74) Friedman, A. E.; Chambron, J.-C.; Sauvage, J.-P.; Turro, N. J.; Barton, J. K. *J. Am. Chem. Soc.* **1990**, *112*, 4960–4962.
- (75) Jenkins, Y.; Friedman, A. E.; Turro, N. J.; Barton, J. K. *Biochemistry* **1992**, *31*, 10809–10816.
- (76) Pyle, A. M.; Rehmman, J. P.; Meshoyrer, R.; Kumar, C. V.; Turro, N. J.; Barton, J. K. *J. Am. Chem. Soc.* **1989**, *111*, 3051–3058.
- (77) Fernandez-Moreira, V.; Thorp-Greenwood, F. L.; Coogan, M. P. *Chem. Commun.* **2010**, *46*, 186–202 and references therein.
- (78) Thorp-Greenwood, F. L.; Coogan, M. P.; Mishra, L.; Kumari, N.; Rai, G.; Saripella, S. *New J. Chem.* **2012**, *36*, 64–72.
- (79) Zhang, A.-G.; Zhang, Y.-Z.; Duan, Z.-M.; Wang, K.-T.; Wei, H.-B.; Bian, Z.-Q.; Huang, C.-H. *Inorg. Chem.* **2011**, *50*, 6425–6436.
- (80) Carter, M. T.; Rodriguez, M.; Bard, A. J. *J. Am. Chem. Soc.* **1989**, *111*, 8901–8911.
- (81) Dalton, S. R.; Glazier, S.; Leung, B.; Sanda Win, S.; Megatalski, C.; Nieter Burgmayer, S. J. *J. Biol. Inorg. Chem.* **2008**, *13*, 1133–1148.
- (82) Kalsbeck, W. A.; Thorp, H. H. *J. Am. Chem. Soc.* **1993**, *115*, 7146–7151.
- (83) Angeles-Boza, A. M.; Bradley, P. M.; Fu, P. K.-L.; Wicke, S. E.; Bacsá, J.; Dunbar, K. R.; Turro, C. *Inorg. Chem.* **2004**, *43*, 8510–8519.
- (84) Nair, R. B.; Teng, E. S.; Kirkland, S. L.; Murphy, C. J. *Inorg. Chem.* **1998**, *37*, 139–141.
- (85) Sun, J.; Wu, S.; Han, Y.; Liu, J.; Ji, L.-N.; Mao, Z.-W. *Inorg. Chem. Commun.* **2008**, *11*, 1382–1384.
- (86) Idziorek, T.; Estaquier, J.; De Bels, F.; Ameisen, J.-C. *J. Immunol. Methods* **1995**, *185*, 249–258.
- (87) Adams, J. M. *Genes Dev.* **2003**, *17*, 2481–2495.
- (88) Li, L.; Wong, Y.-S.; Chen, T.; Fan, C.; Zheng, W. *Dalton Trans.* **2012**, *41*, 1138–1141.
- (89) Gottlieb, H. E.; Kotlyar, V.; Nudelman, A. *J. Org. Chem.* **1997**, *62*, 7512–7515.
- (90) *SHELXS97: Program for Crystal Structure solution*; Sheldrick, G. M., Ed.; University of Göttingen: Göttingen, Germany, 1997.
- (91) *SHELXL97: Program for Crystal Structure Refinement*; Sheldrick, G. M., Ed.; University of Göttingen: Göttingen, Germany, 1997.